American Mineralogist, Volume 89, pages 74–84, 2004

Pyribole evolution during tremolite synthesis from oxides

KRASSIMIR N. BOZHILOV,[1,*] DAVID M. JENKINS,[2] AND DAVID R. VEBLEN[3]

[1]Institute of Geophysics and Planetary Physics, University of California, Riverside, California 92521, U.S.A.
[2]Department of Geological Sciences, Binghamton University, Binghamton, New York 13902, U.S.A.
[3]Department of Earth and Planetary Sciences, The Johns Hopkins University, Baltimore, Maryland 21218, U.S.A.

ABSTRACT

The formation mechanisms of tremolite in a time series of hydrothermal experiments at 850 °C and 6.1 kbar were studied using transmission electron microscopy (TEM), analytical TEM, and X-ray diffraction. The starting materials were unseeded mixtures of reagent-grade oxides. After the first 8 min of reaction, the synthesis products were diopside, enstatite, clinoenstatite, quartz, and minor *C*-centered and primitive monoclinic amphibole (13 wt% total). The compositions of the first-formed amphiboles vary considerably, from essentially pure cummingtonite (Ca/Mg = 0) to nearly ideal tremolite (Ca/Mg = 0.4). Three groupings of amphiboles with successively higher Ca/Mg ratios were identified, respectively 0.1, 0.22, and 0.35. Over a period of 97 h, the proportions of Mg-rich amphibole gradually decrease, and the average Ca/Mg ratios of all amphiboles steadily increase from about 0.22 to 0.35. Other changes include: (1) a decrease in the aspect ratio of amphibole crystals with increasing time; (2) a decrease in the number of non-amphibole chain multiplicity faults (CMFs), from early A'(2) values as low as 0.81 to a final value of 0.94; and (3) a distinct change in the rate of amphibole growth after 1 h of synthesis. These observations suggest that two mechanisms of amphibole formation are dominant: (1) formation of pyroxene modules with subsequent hydration and arrangement into the double-chain amphibole structure and (2) direct nucleation and growth of amphibole from hydrothermal solution. A third mechanism involving formation of talc-like modules, followed by their breakdown into double-chain modules, incorporation of Ca, and ordering into the amphibole structure, may also occur but probably only at the lamellar or unit-cell scale, because these syntheses were performed outside the stability field of talc.

INTRODUCTION

Compositional deviations of biopyriboles from their end-member compositions are important for assessing their thermodynamic and other properties. Compositional variations in biopyriboles can arise from two different phenomena: (1) true solid solution or (2) structural defects in the form of precipitates (exsolution lamellae), chain-multiplicity faults (CMFs), or other defects. Failure to recognize correctly the cause of compositional variations can lead to erroneous interpretations of experimental thermodynamic or petrologic data.

Synthesis of tremolite, $Ca_2Mg_5Si_8O_{22}(OH)_2$, has been exploited extensively for several decades to shed light on the thermodynamic properties of one of the simplest amphibole compositions. The studies of Boyd (1959), Troll and Gilbert (1972), Robie and Stout (1963), Kiseleva and Ogorodova (1984), Skippen and McKinstry (1985), Jenkins (1987), Welch (1987), Graham et al. (1989), Jenkins and Clare (1990), Jenkins et al. (1991), Welch and Pawley (1991), Pawley et al. (1993), Maresch et al. (1994), Zimmerman et al. (1996), Chernosky et al. (1998), and Gottschalk et al. (1999) have clarified many aspects of the thermodynamics and synthesis of tremolite. Still, there are unanswered questions about the range and causes of Mg enrichment in tremolite, the types of structural defects present in synthetic tremolite, the mechanisms of defect formation, and the reasons for almost universally incomplete tremolite yields during synthesis.

Tremolite (Hawthorne 1983; Yang and Evans 1996) is a member of the amphibole family, which in turn is part of the larger group of biopyriboles (Thompson 1978, 1981; Veblen 1981). The biopyriboles are a group of related chain- and sheet-silicate mineral structures, which can be represented as being built of different proportions of pyroxene and mica (or talc) modules. In biopyriboles crystallizing in the system CaO-MgO-SiO_2-H_2O, limited substitution of Ca by Mg is commonly observed in the pyroxene and amphibole families. Numerous studies (Boyd 1959; Metz 1967, 1976; Hewitt 1975; Yin and Greenwood 1983; Jenkins 1983, 1987; Pawley et al. 1993) have reported synthetic and natural tremolite compositions with about 3 to 10 mol% cummingtonite (Cm) component, $Mg_2Mg_5Si_8O_{22}(OH)_2$, which typically has been interpreted as being in solid solution. Alternatively, the observed compositional shift toward Cm might result from the presence of defects. Biopyriboles commonly contain structural defects that can be described as errors in the chain width or multiplicity, designated "chain-multiplicity faults" (Hutchison et al. 1975; Veblen et al. 1977; Maresch and Czank 1983, 1988). In biopyriboles, multiplicity is defined as the number of tetrahedral subchains comprising the full tetrahedral chain. Thus, the pyroxene structure has multiplicity one, amphibole has multiplicity two, jimthompsonite three, and mica (or talc)

*E-mail: bozhilov@ucr.edu

infinity. The TEM studies by Ahn et al. (1991), Bozhilov et al. (1993, 1994), and Maresch et al. (1994) have found that CMFs are common structural defects in synthetic tremolite.

Maresch et al. (1994) concluded that the compositional shifts of the ideal Ca/Mg ratio of synthetic tremolite from 0.4 to 0.37–0.34 result primarily from the presence of CMFs. They attributed only about 2 mol% of the Mg enrichment to true solid solution. This interpretation differs from that proposed in some of the studies mentioned above. Thus, further work is required to explain and clarify the cause of variations in Ca and Mg of synthetic tremolite and the mechanisms of crystal growth in amphibole synthesis experiments.

In the present study, we have applied TEM methods for structural and compositional characterization of the crystallization products of a time series of hydrothermal synthesis experiments performed in the tremolite stability field. The results not only shed light on the structural mechanisms of Mg enrichment in tremolite, but also explain why the synthesis of pure, end-member tremolite is so difficult.

Experimental methods

Synthesis techniques

The starting phases used in this study were synthesized hydrothermally from mixtures of reagent-grade $CaCO_3$, SiO_2 (amorphous), and MgO, mixed in the molar ratios 1:4.44:2.89, corresponding theoretically to 10% solid solution of cummingtonite in tremolite. All of the experiments were conducted at 850 ± 7 °C and 6.10 ± 0.05 kbar. Each mixture was sealed in either a gold or platinum capsule with about 30 wt% water. Prior to sealing, the CO_2 was driven out of the $CaCO_3$ by heating briefly for 30 s in air at 900 °C. A slight excess of quartz was added to help ensure silica saturation and to prevent the incongruent dissolution of tremolite (Jenkins 1987). Time series synthesis experiments were performed at the above conditions with durations of 8 min and 1.0, 4.0, 12.2, 20.0, 28.3, 36.0, and 97.3 h.

X-ray diffraction (XRD)

The starting materials and experimental products were examined with XRD both for phase identification and for quantitative analysis of the proportions of phases present. All experimental materials were analyzed with a Norelco X-ray diffractometer using Ni-filtered Cu$K\alpha$ radiation. The proportions of phases present in each experiment were determined by the method of Rietveld XRD refinement applied to the central portions (18–40 °2Θ) of the digitized powder patterns. Refinements were done with the upgraded program DBWS-9807 (Young et al. 1995) using the single-crystal structure data of Hawthorne and Grundy (1976) for tremolite, Levien and Prewitt (1981) for diopside, Sasaki et al. (1982) for enstatite, Lager et al. (1982) for quartz, and Yang and Hirschmann (1995) for $P2_1/m$ cummingtonite. A Pseudo-Voigt peak profile was refined for quartz from the most quartz-rich sample and then applied uniformly to all of the phases. In addition to the scale factors, which were refined for all phases, the cell dimensions were refined for major phases (>10 wt%). For patterns in which tremolitic amphibole was a major phase (experiments >12 h), the Ca and Mg content of the M4 site was refined along with the degree of preferred orientation of the $hk0$ reflections, as modeled by the Rietveld-Toraya function (Young et al. 1995). Weight percentages of the phases were calculated from the refined scale factors, unit-cell volumes, molecular weights, and unit-cell contents of each phase, as described by Snyder and Bish (1989). The uncertainty in the proportion of a phase is dominated by the uncertainty in the refined scale factor.

Transmission electron microscopy (TEM)

All samples were examined at an accelerating voltage of 120 kV using a Philips 420ST TEM (spherical and chromatic aberration coefficients C_s = 1.2 mm and C_c = 1.2 mm). The fine-grained synthesis run products were suspended in ethyl alcohol without grinding, and after 5 min agitation with an ultrasonic cleaner were deposited onto holey carbon films supported by copper mesh grids. High-resolution TEM (HRTEM) images were obtained with a 100 µm objective aperture and a beam convergence angle of about 9 mrad. Interpretation of images was based on comparisons of experimental and simulated images using the EMS software package for the simulation of HRTEM images (Stadelmann 1987), as well as by comparison with results of Veblen et al. (1977).

Analytical TEM

Analytical electron microscopy was used to determine chemical compositions of the starting and product phases. The analyses were obtained using energy-dispersive X-ray spectroscopy (EDS) at 120 kV in the Philips 420ST TEM, with a Link Li-drifted silicon detector (135 nm FWHM peak resolution at Mn$K\alpha$) and a Link 4020 pulse processor. The signal was discriminated and processed with a 4pi Analysis 1260 SpringBoard analyzer, Spectral Engine software, and the DTSA software package (Fiori et al. 1994). The analyses were obtained from thin particles or particle edges, with an effective take-off angle of 20°, probe size between 20 and 200 nm, and they were reduced following the procedures and standards of Livi and Veblen (1987). Because of the generally low precision of EDS analysis in a TEM (typically ≥2% relative for major elements), many crystals were analyzed to improve the statistical base. Analyses of about 50 to 60 particles were obtained for each synthesis experiment.

Results

XRD

The phases identified in the different time-series experiments and their relative proportions are presented in Table 1. In general, crystallization starts with the predominant formation of diopside. After 4 h, tremolite becomes the dominant phase, with enstatite essentially disappearing after the 20 h treatment. After a total crystallization time of 97.3 h, the yield of amphibole is slightly less than 100% with about 2% diopside remaining. Each experimental charge was also checked for the spontaneous growth of talc by looking for the 002 reflection, which was not observed.

Because monoclinic amphiboles with a primitive as well as a *C*-centered lattice were observed in this study (see below), attempts were made to determine the presence of both cummingtonite ($P2_1/m$) and tremolite ($C2/m$) in the X-ray pattern by Rietveld refinement. The large degree of overlap in the patterns of these two monoclinic amphiboles produces large uncertainties in their relative proportions. In addition, there is a large variation in the Ca/Mg ratio of amphibole during its formation, as discussed below, which further blurs the distinction between cummingtonite and tremolite. For these reasons only the total amphibole content is reported in Table 1. Despite these limitations, the refinements indicate that the first experiment had the highest amount (~10 wt%) of cummingtonite, and subsequent experiments showed a steady decrease until no statistically significant cummingtonite could be determined from the pattern after 12 hours.

Figure 1 shows the fraction of (total) amphibole formation with time based on the Rietveld refinements. Except for the 20

Table 1. Phase proportions (wt%) deduced from Rietveld refinement of the X-ray powder diffraction patterns

Sample	Cumulative time	Diopside	Enstatite	Amphibole	Quartz
23-11-1	8 min	40(1)	12(1)	30(3)	18(1)
23-7-1	1.0 h	31(1)	20(1)	34(2)	14(1)
23-7-2	4.0 h	20(1)	14(1)	50(2)	16(1)
23-7-3	12.2 h	8.9(2)	3.7(2)	87(1)	0
23-11-2	20.0 h	10.6(2)	4.6(3)	80(1)	4.1(3)
23-7-4	28.3 h	3.3(2)	1.1(2)	96(1)	0
23-11-3	36.0 h	2.8(2)	1.2(2)	95(1)	1.3(3)
23-7-5	97.3 h	1.6(2)	0	98(1)	0

Notes: Uncertainties (1 σ) in the last digit are indicated in parentheses.

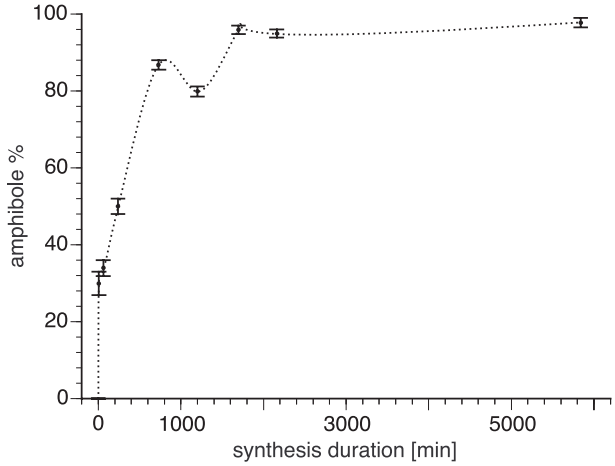

FIGURE 1. Evolution of the mass fraction (concentration) of amphibole with time determined by XRD Rietveld refinement.

h (1200 min) experiment, there is a consistent increase in the proportion of amphibole with time. The deviation observed for the 20 h experiment may be related to the unexpected pressure drop (by 0.8 kbar) from a ruptured monitoring thermocouple in the latter half of this particular experiment, which may have reduced the tremolite crystallization rate.

For very small (<1 μm wide) amphibole crystals, the 151 reflection is stronger than the 310 reflection as is expected for the case of no preferred orientation (i.e., Borg and Smith 1969). With continued experimental treatment, the 310 displays a systematic increase in its intensity relative to the 151. This behavior is attributed here to grain coarsening (Ostwald ripening), with a resultant increase in the preferred orientation that is typically obtained with flat-plate XRD mounts. It is noted that including the preferred orientation term in the Rietveld refinements significantly improved the agreement index, although it did not completely compensate for this effect.

Refinement of the Ca and Mg content of the M4 site in tremolite was attempted for experimental charges with high (>80 wt%) amphibole content. The refined Ca contents ranged from 1.44 to 1.89 ± 0.05 Ca atoms per formula unit (apfu) and showed no systematic variation with treatment duration, indicating that the X-ray patterns obtained in this study were not particularly sensitive to the Ca and Mg content at the M4 site. Similarly, the cation occupancy at the M4 site was found to have little effect on the derived proportions of phases for experiments with <50 wt% amphibole by comparing the results obtained for tremolite for which its M4 content was fixed at either pure Mg or pure Ca.

TEM

Morphology and size distribution. The morphology and grain-size distributions of the run products were determined from TEM micrographs. Figure 2 shows typical morphologies after 8 min (a), and 97 h (b), respectively. The diopside has an equant shape, the enstatite has prismatic habit with an aspect ratio between 3 and 10, and quartz crystals have irregular shapes and variable sizes. The aspect ratio of amphibole crystals was determined by measuring from TEM micrographs the width and

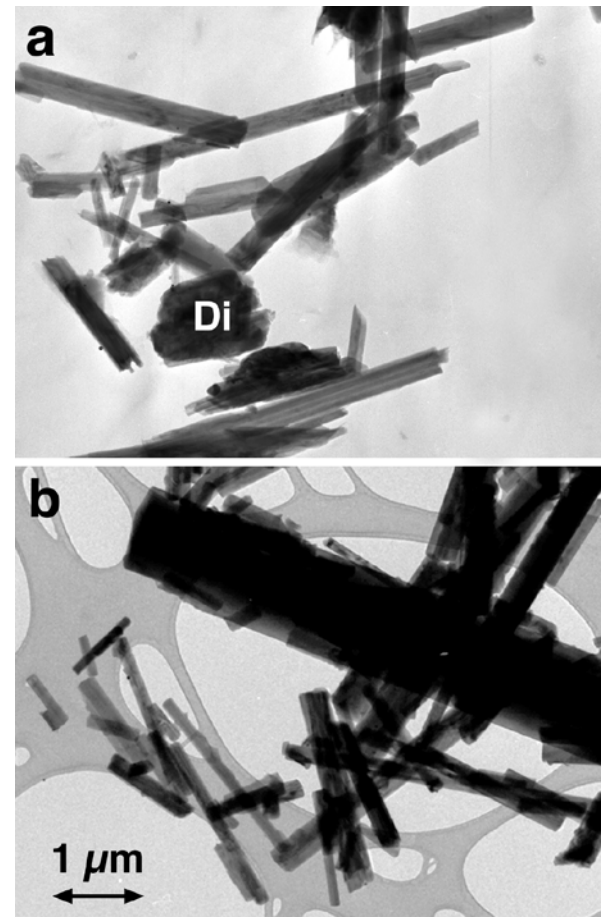

FIGURE 2. TEM micrographs showing the morphology of the product phases after different synthesis durations: **(A)** 8 min and **(B)** 97 h. Note the two distinct amphibole generations from the 97 h experiment.

length of about 50 individual crystals from each experiment with precision in measurement of individual dimensions of ±5 nm and accuracy of ±3%, which results in an error of about ±6% in aspect ratio determinations. The amphibole crystals grow as long, thin fibers with an average aspect ratio of 11.3 ± 4.2 (1 σ) during the first 4 h of treatment. In the final stages (after 36 h), the average aspect ratio of amphibole decreases to 8.2 ± 3.7. The typical amphibole length varies between 0.5 and 3 μm with an average of 2.4 ± 1.4 μm, and the width varies between 0.1 and 0.5 μm or slightly larger, with an average width of 0.21 ± 0.11 μm. Two crystal types with different widths develop in the later growth stages, after about 28 h: one having an average width of 0.16 ± 0.05 μm and the other having a width greater than 0.5 μm (average width 0.8 ± 0.5 μm). The pronounced difference in diopside and amphibole widths along the **b** axis suggests that tremolite does not directly replace diopside, or that the replacement is at least a more subtle process. Overall, the crystal size data suggest that the process of amphibole formation is complex and goes through multiple steps of phase nucleation, dissolution, re-precipitation, and grain coarsening, as discussed below.

Structure and defects. Phase identification by TEM was based on both selected-area electron diffraction (SAED) and

TABLE 2. Average compositions of pyroxenes observed in all synthesis experiments based on EDS analyses in the TEM

Phase		MgO wt%	CaO wt%	SiO_2 wt%	Mg apfu	Ca apfu	Si apfu	Analyses
Enstatite	average	39.25	1.93	58.82	1.98	0.07	1.99	9
	st. dev.	0.64	0.15	0.45				
	error %	2.63	9.21	2.33				
Diopside	average	18.91	25.54	55.54	1.02	0.99	2.01	29
	st. dev.	0.71	0.68	0.52				
	error %	3.54	4.20	1.84				

Notes: The pyroxene formulas are calculated assuming 6 oxygen atoms per formula unit (apfu). The standard deviation value is based on the spread of the data from multiple analyses. Under "error" are listed the uncertainties in measuring the X-ray peak intensities due to counting statistics.

EDS. All phases observed by powder XRD were confirmed by electron diffraction. The diopside, enstatite, and quartz were easily distinguished by SAED patterns and composition (Table 2).

Two distinct amphibole phases were identified based on SAED patterns. The first one corresponds to tremolite with the well-known *C*2/*m* structure. The second one is a primitive monoclinic amphibole. For this primitive monoclinic amphibole, the SAED patterns contained reflections with $h+k$ = odd, thus proving that the *C*-centering is violated. The SAED patterns were indexed with a monoclinic *P* lattice. Obtaining SAED patterns along several zone axes from individual crystals with reflections violating the *C*-centering extinction rules unambiguously rejects the presence of orthorhombic amphibole. The intensities of the reflections violating the *C*-centering vary from crystal to crystal. This finding suggests different degrees of structural ordering. Imaging by HRTEM showed that *C*-centered and primitive domains are intimately and coherently intergrown (Fig. 3).

The compositions of both centered and primitive amphiboles lie on the join tremolite–cummingtonite (Tr–Cm) and are clustered around three compositionally distinct types: (1) cummingtonite (Cm) with Ca/Mg ratio below 0.1; (2) intermediate tremolitic amphibole (Cm-TrI), with high Cm component and a Ca/Mg ratio between 0.15 and 0.3; and (3) tremolitic amphibole (Cm-TrII), with limited Cm component and a Ca/Mg ratio between 0.3 and 0.4 (Table 3). *C*-centered amphiboles were observed for all three compositions whereas the primitive amphiboles are more Mg-rich than the *C*-centered ones and compositionally belong either to Cm or Cm-TrI types (Ca/Mg ratio less than 0.3). Both the primitive and *C*-centered amphiboles persist throughout all time-series experiments. After the first 20 h of treatment, the general tendency is toward a decrease in the number of primitive monoclinic amphibole particles, compared to those with space group *C*2/*m*.

The HRTEM micrographs of amphibole and pyroxene confirmed the presence of intergrown polysomatic slabs (Fig. 4). By imaging the amphibole crystals down the [100] or other [*h*0*l*] directions, the silicate chain width can be determined directly, and the presence of CMFs can be documented. The fractions of tetrahedral chains with different multiplicities were determined by relating the total number of silicate tetrahedral chains to the

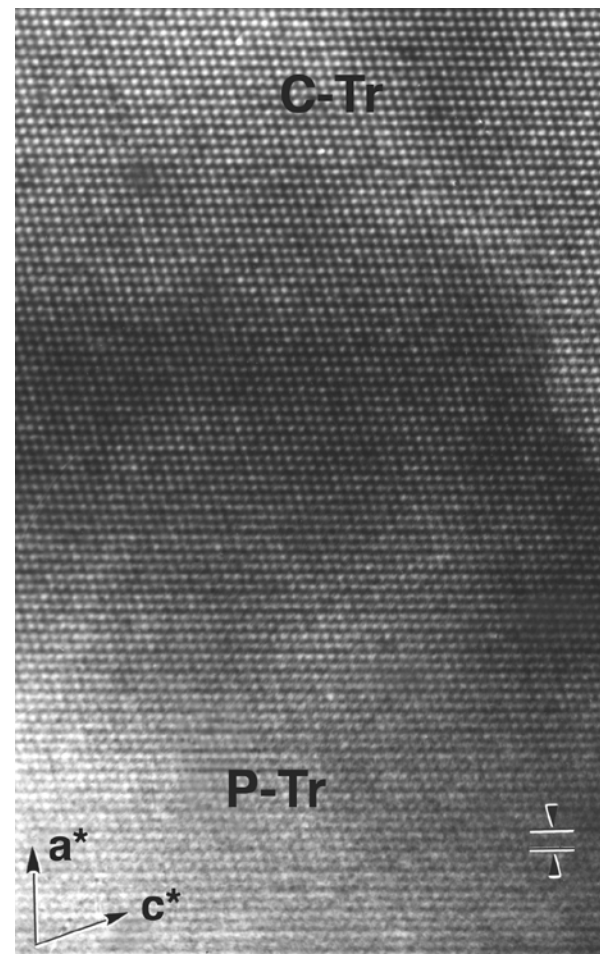

FIGURE 3. HRTEM image of amphibole down [010]. Coherently intergrown domains of *C*-centered (C-Tr) and primitive (P-Tr) tremolitic amphibole are visualized. The doubled periodicity in the lattice fringes perpendicular to **a*** in the primitive part of the structure is due to the absence of *C*-centering translational symmetry. The periodicity of 9.5 Å is marked on the image.

TABLE 3. Average compositions (wt%) and structural formula (apfu) on the basis of 23 O atoms of the three types of amphiboles Cm, Cm-TrI, and Cm-TrII from different synthesis duration experiments based on normalized TEM-EDS analyses

Phase		Composition at time *t*, min				
		8	60	240	1200	5950
Cm	MgO	33.7(1.2)	33.9(1.1)	31.7(1.2)*		
	CaO	4.4(0.2)	3.1(0.3)	6.2(0.3)		
	SiO_2	61.9(0.9)	63.0(1.1)	62.1(0.9)		
	Mg	6.49	6.43	6.07		
	Ca	0.61	0.42	0.85		
	Si	7.99	8.01	7.98		
	Ca/Mg	0.094	0.065	0.140		
	Fraction	0.12	0.06	0.04		
	n	6	3	2		
Cm-TrI	MgO	30.2(1.2)	29.5(1.2)	28.3(1.1)	28.0(1.1)	27.9(1.1)
	CaO	8.7(0.3)	9.4(0.3)	10.3(0.3)	10.5(0.28)	11.3(0.3)
	SiO_2	61.1(0.9)	61.0(1.0)	61.4(1.1)	61.5(0.9)	60.8(1.0)
	Mg	5.88	5.78	5.49	5.43	5.49
	Ca	1.21	1.33	1.44	1.46	1.59
	Si	7.97	8.02	7.99	7.98	8.01
	Ca/Mg	0.206	0.230	0.262	0.269	0.290
	Fraction	0.59	0.35	0.38	0.28	0.12
	n	30	18	19	14	10
Cm-TrII	MgO	27.4(1.0)	26.1(1.1)	26.4(1.2)	25.9(1.1)	25.7(1.1)
	CaO	12.0(0.3)	13.2(0.3)	13.0(0.3)	13.2(0.3)	13.6(0.3)
	SiO_2	60.6(1.0)	60.7(1.1)	60.6(1.0)	60.9(0.9)	60.4(0.9)
	Mg	5.39	5.10	5.19	5.06	5.13
	Ca	1.70	1.85	1.83	1.86	1.95
	Si	8.00	7.96	7.99	7.98	8.01
	Ca/Mg	0.315	0.363	0.353	0.368	0.380
	Fraction	0.29	0.59	0.58	0.72	0.88
	n	14	30	29	36	44

Notes: The standard deviation is replaced by the range for the Cm from the 240 min experiment. The relative mass fraction (Fraction) of the amphibole type at a given time is indicated. Uncertainties (1 σ) for the compositions are based on analyses of multiple grains (n).

absolute number of those having a particular multiplicity (i), which is defined as the A'(i) value (Maresch and Czank 1988; Ahn et al. 1991). Because the number of chains with multiplicities greater than 3 was generally low, and the occurrence of chains with multiplicity greater than 6 was extremely rare, calculation of the Cm component was simplified in this study by treating all CMFs greater than 3 as though they were 6 (Table 4). For each time-series experiment, the CMF density was determined for about 7 to 10 crystals. The majority of amphibole crystals have A'(2) values above 0.9 (Table 4). The highest defect densities in amphibole are observed during the initial 4 h of synthesis, and the defect density drops steadily with run time. However, some defects persist even in the final run.

Chemical analyses of individual grains studied by HRTEM were also obtained by EDS (Table 4). The Cm component in the amphiboles was calculated by first using the observed Ca/Mg ratio and then correcting for the Mg enrichment due to CMFs. Unfortunately, the small thicknesses of the individual anomalous pyribole lamellae (usually 0.5–2 nm) precluded direct determination of their compositions. Only large (>10 nm) single-chain slabs could be analyzed reliably, and they always gave the composition of diopside. All other intergrown slabs were assumed to have Ca end-member compositions, namely $CaMgSi_2O_6$ (diopside) for single chains, $Ca_2Mg_8Si_{12}O_{32}(OH)_4$, for triple chains, and $Ca_2Mg_{17}Si_{24}O_{62}(OH)_{10}$ for sextuple chains. It should be emphasized that, because of the small thicknesses of the CMF lamellae (usually 1–3 half unit cells, i.e., 1–3 silicate chains wide), the actual Cm component in the double-chain parts of the crystal will differ on average less than 1% from the values listed in Table 4, even if the intergrown slabs have pure Mg end-member compositions.

General observations

The results suggest that the whole experiment can be divided into three intervals: starting stage (0–1 h), intermediate stage (1–36 h), and final stage (36–97 h).

Starting stage (8 min and 1 h syntheses). At the very first stage of reaction, the oxide starting mixture reacts quickly to the

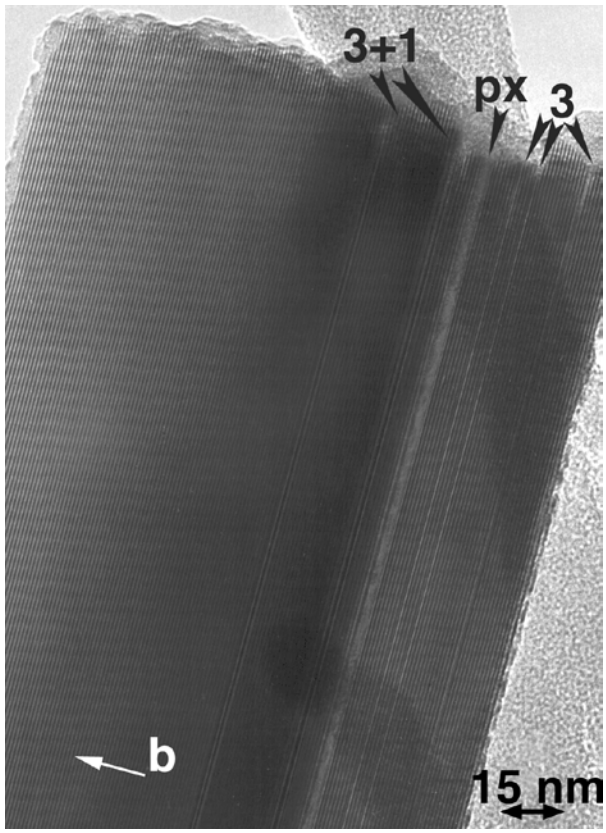

FIGURE 4. Tremolite crystal from the 12 h experiment showing typical concentrations of CMFs. Isolated triple (3) and single (1) chains as well as a pyroxene slab six chains wide are visualized. They transect the entire amphibole crystal without any terminations. The measured Ca/Mg ratio of the whole crystal is 0.35, with an A'(2) value of 0.94. This corresponds to 9.25% Cm component as solid solution, of which only 0.85% can be attributed to the CMFs. Any horizontal periodicity is an artifact of the digitizing process.

TABLE 4. Average CMF density and the corresponding Cm component in amphibole for synthesis experiments with different durations

Duration	A'(1)	A'(2)	A'(3)	A'(i)*	Ca/Mg (EDS)	% Cm due to CMFs	% Cm total
8 min	0.08	0.88	0.03	0.01	0.3	-0.43	19.63
1.0 h	0.09	0.81	0.06	0.03	0.305	3.05	18.2
4.0 h	0.02	0.93	0.04	0.01	0.34	2.51	11.2
12.2 h	0.02	0.92	0.05	0.01	0.338	2.9	11.6
20.0 h	0.015	0.935	0.04	0.005	0.33	1.55	13.1
28.3 h	0.04	0.91	0.03	0.02	0.35	2.9	9.3
36.0 h	0.02	0.90	0.06	0.02	0.34	4.89	11.2
97.3 h	0.01	0.94	0.045	0.005	0.35	2.3	9.27

* A'(i) is average of all CMFs larger than 3. For calculation of the Cm component, a value of A'(6) is assumed for all CMFs larger than 3.

crystalline assemblage diopside, enstatite, clinoenstatite, *C* and *P* amphiboles, and quartz, all present at micrometer and submicrometer sizes. Diopside crystals are dominant and have perfect crystalline structure. No replacement structures were observed in diopside. Enstatite is present as elongated, prismatic crystals. Some of them show fiber-like habit with aspect ratios of 50 or more. The density of CMFs in enstatite is low, with isolated defects one or two silicate double chains wide running the entire

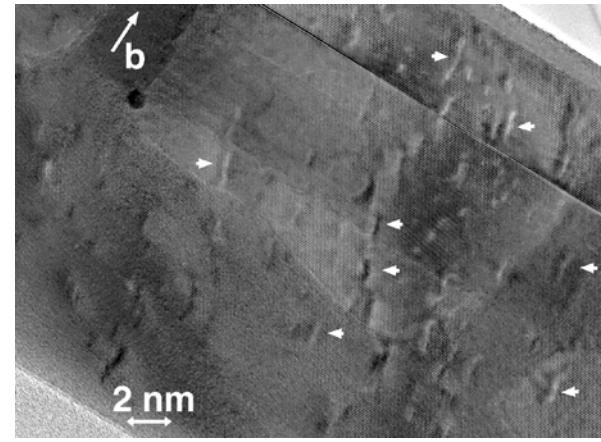

FIGURE 5. HRTEM micrograph of an enstatite ($Mg_{1.9}Ca_{0.1}Si_2O_6$) crystal from the 8 min experiment. Nanometer-sized segregations (Guinier-Preston zones), shown by white arrows, are present. A stacking fault is visible as a dark line.

crystal length parallel to the **c** axis. Guinier-Preston zones about 0.5 nm wide and 10 nm long (Fig. 5), which are characteristic of the initial stages of exsolution, are present in some enstatite crystals. The compositions of the individual zones could not be determined due to their small size. The presence of about 0.1–0.3 Ca per 6-oxygen formula unit in such crystals suggests the possible exsolution of Ca-rich precipitates.

Amphibole forms elongated crystals with aspect ratios between 5 and 10, and both *P*- and *C*-centered monoclinic lattice types are observed. The abundance of amphibole increases with synthesis duration. The CMF density in the amphiboles is high, and single-chain slabs are the most abundant defects, with average A'(2) value of 0.845 (Table 4). The single-chain slabs are typically about 3 to 5 silicate chains wide and run the entire length of the crystal parallel to the **c** axis (Fig. 6). Terminations of CMFs within a crystal are rare. Triple and wider chains are not abundant or, if present, they form isolated slabs that are generally only one multiple silicate chain wide.

Topotactic intergrowths between diopside and primitive monoclinic amphibole are observed, where [100] of diopside is parallel to $[10\bar{1}]$ of amphibole. Both the presence of a coherent phase boundary and the large sizes of the amphibole slabs suggest simultaneous growth of diopside and amphibole. Thin amphibole slabs (Fig. 7a) run the entire length of the diopside crystals parallel to the silicate chains. A dissolution process is also obvious between individual amphibole slabs (Fig. 7b), where the pyroxene portion of the composite crystal is noticeably embayed.

Intermediate stage (4, 12, 20, 28, and 36 h experiments). The abundance of amphibole increases continuously with time, while its aspect ratio decreases. Particularly noticeable is the decreasing abundance of cummingtonite crystals, which have become rare in the 4 h experiment and almost disappear after 20 h synthesis. With increasing time, the amount of diopside decreases slowly, and enstatite is almost entirely gone after 20 h of treatment. The average thickness of the amphibole grains increases slightly, compared with those from shorter runs. Violations of the *C*-centering were observed for fewer than 7% of

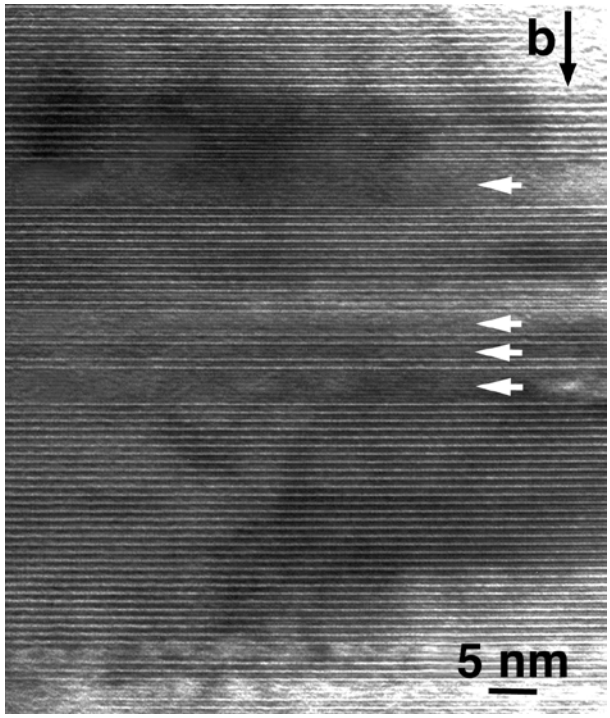

FIGURE 6. HRTEM micrograph of amphibole down [100]. Double-chain domains are coherently intergrown with single-chain lamellae (marked with white arrows) having diopside composition. This amphibole crystal shows higher than average defect density. The pyroxene lamellae transect the whole crystal without showing distinct replacement fronts.

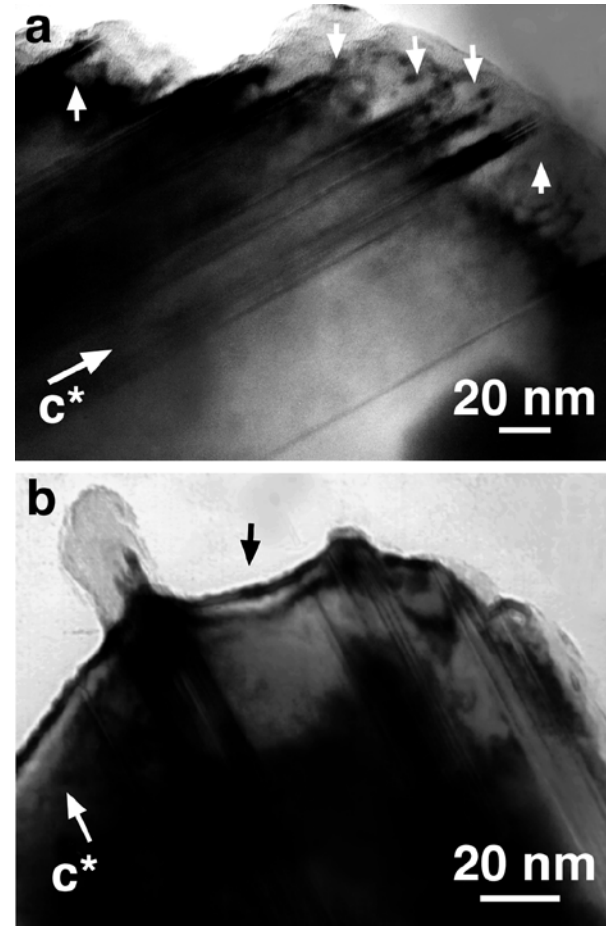

FIGURE 7. (a) Electron micrograph of a diopside crystal exhibiting pronounced development of double-chain slabs (short white arrows) by topotactic nucleation and growth. **(b)** Dissolution of the pyroxene part of the crystal (black arrow) occurs simultaneously with double-chain slab growth, suggesting a lack of direct topotactic replacement of entire diopside crystals by amphibole.

the 52 amphibole crystals examined with SAED. The examined diopside crystals do not contain CMFs or extensive intergrown amphibole slabs as observed in the shorter duration experiments. After 28 h of treatment, two generations of amphibole grains were observed: one with sizes along the **b** axis between 0.05 and 0.2 μm and one with sizes ≥0.5 μm. The dimensions of the amphibole grains perpendicular to the **c*** axis (typically 0.1–0.5 μm) are significantly smaller than the corresponding dimensions of diopside (~2 μm), which suggests that direct conversion of diopside to tremolite by overgrowth or across broad conversion fronts plays a relatively minor role (cf., Maresch et al. 1994). The average A'(2) values of amphibole crystals range from 0.90 to 0.93 for different experiments (Table 4). The CMFs are present as lamellae 1 to 3 multiple silicate chains thick. Terminations of CMFs within the crystals are rare, and triple-chain slabs are the most abundant CMFs. Defect-free amphibole grains with Ca/Mg ratios below 0.4 were observed for all experiments in this intermediate stage.

Final stage (97 h experiment). The final products consist of amphibole with minor amounts of diopside. The remaining diopside crystals are relatively large, averaging about 2 μm perpendicular to the **c** axis. Amphibole crystals continue to occur in two crystal size ranges: those that are relatively thick (~1 μm) with aspect ratios ≥10, and those that are relatively thin (0.02–0.2 μm) with typical aspect ratios of about 5 (Fig. 2b). These two crystal size populations may be evidence of dissolution and regrowth, producing grain coarsening among the amphibole crystals. Cummingtonite crystals were not observed. The average A'(2) value of amphibole is 0.94. The CMFs are predominantly isolated triple-chain lamellae one to two silicate chains thick.

Chemical composition variation.

Diopside and enstatite show limited compositional variation for all of the experiments (Table 2). The diopside Ca/Mg ratio varies from 0.9 to 1.0 (ideal = 1). Enstatite crystals were observed to incorporate up to 0.3 Ca ions per 6-oxygen formula unit. No systematic variation was observed in the average diopside composition for different run times. The amphibole, in contrast, showed significant variations in composition (Fig. 8a). With increasing synthesis duration, the spread in composition decreases, and the average value of the Ca/Mg ratio increases from 0.22 in the 8 min experiment to 0.357 after 97 h of treatment. As already mentioned, three compositionally distinct types of amphibole were observed: Cm, Cm-TrI, and Cm-TrII (Table 3). Figure 8b shows variations in the abundances of the three different types of amphibole for the same experiments for which EDS analyses of

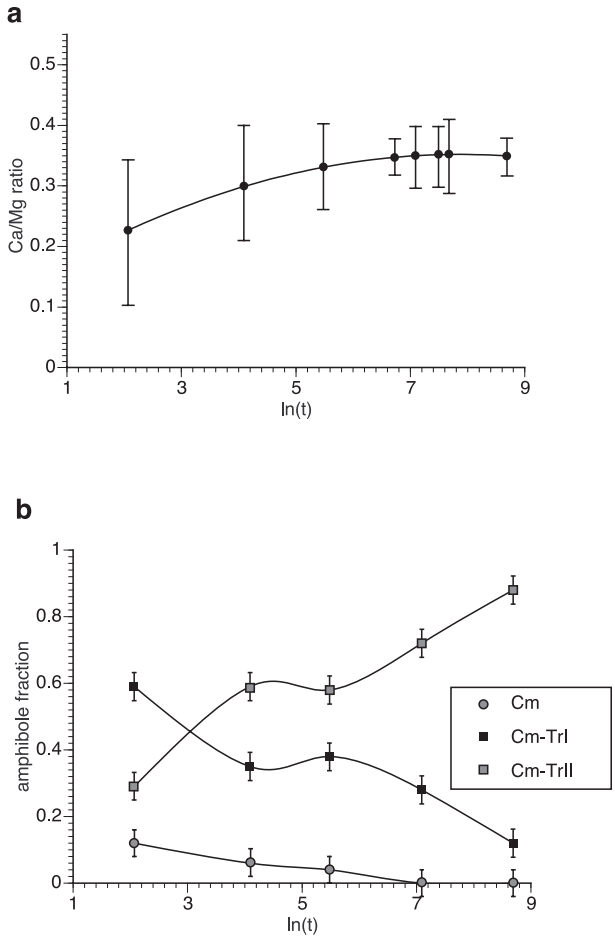

FIGURE 8. (**a**) Plot of the average Ca/Mg ratio of amphibole crystals obtained by EDS analyses vs. the natural log of synthesis duration (min). The error bars represent the standard deviation. Note the large spread of compositions for the initial stages of growth. **(b)** Change of the fraction of the three types of amphibole compositions vs. the natural log of time (min).

individual particles were obtained. In the beginning, cummingtonite and Cm-rich tremolitic amphibole (Cm-TrI) are present in significant amounts, but they are substantially reduced after 4 h of treatment. In the 1 h experiment, the fraction of Cm-TrI has decreased considerably. In the final stages, the amount of amphibole with Ca/Mg ratios below 0.3 has decreased to about 12%. Some amphibole grains with Ca/Mg ratio above 0.4 were observed; these are due to the incorporation of single-chain slabs of diopside composition. There are also individual grains of amphibole lacking any CMFs but with Ca/Mg ratios between 0.33 and 0.38, which correspond to levels of Cm component in true solid solution of 13.1 and 3.6 mol%, respectively.

There is no general correlation between the presence of CMFs and variations in the Ca/Mg ratio of the amphibole. The compositions of both *C*-centered and primitive amphiboles lie on the tremolite–cummingtonite join (Tr–Cm). The *C*-centered tremolitic amphibole incorporates from 0 to approximately 22 mol% of the Cm component. Most of the primitive amphiboles have Ca/Mg ratios at or below 0.3 (20 mol% Cm), but exceptions to this rule are not rare. On average, the primitive amphibole is more Mg-rich than the *C*-centered amphibole. Two compositional groups of primitive amphibole are observed. The first one is almost pure cummingtonite, with very low Ca content and a Tr component from 5 to 10%, whereas the second group is relatively Ca-rich amphibole, with a Tr component between 60 and 90%.

DISCUSSION

Kinetics and mechanism of growth

The mechanisms and kinetics of growth of many heterogeneous reactions can be estimated using the well-known Johnson–Mehl–Avrami rate law (Christian 1975):

$$y = 1 - \exp(-kt)^n \quad (1)$$

where y is the fraction of the process completed, k is a rate constant proportional to the activation energy, t is time, and n is an exponential term (reaction order) that depends on the mechanism of the reaction. A plot of $\ln\{\ln[1/(1 - y)]\}$ against $\ln(t)$ should give a straight line with slope n. Such a plot is shown in Figure 9 using the fraction of amphibole formed (y) from Table 1. It is evident that there is a change in reaction order (slope) at the 1 h experiment (which is *not* the experiment with the failed thermocouple) and that amphibole probably forms by more than one mechanism.

We can interpret both the TEM observations and the analysis of reaction rates in the following way. The initial crystallization process is very fast. After only 8 min, the starting oxide mixture is completely transformed into a mixture of pyroxenes, amphibole, and quartz. Diopside has the fastest growth rate and is the dominant phase in the initial stage of growth (up to 1 h). The presence of numerous small amphibole crystals, which increase in absolute number and relative abundance while at the same time preserving their small sizes, is evidence for constant amphibole nucleation in the initial growth stages. A change in amphibole growth mechanism starts after 1 h, as suggested by the break in slope of the reaction rate curve, and begins to produce two populations of amphibole particles with different widths caused by a coarsening of some of the grains. Grain coarsening becomes the dominant growth mechanism after 28 h, at which time one can readily document two distinct populations of amphibole grain widths.

Based on the observations from the initial crystallization experiments, single-chain formation is the most important process during the initial stages of crystallization. Formation of talc as a separate phase does not occur in this study, because the temperature of synthesis (850 °C) is about 80 °C above the thermal breakdown boundary of talc at 6 kbar (Aranovich and Newton 1999). Formation of talc modules at the unit-cell scale is also very limited. Even after only 8 min of crystallization, when metastable phases would be most likely to appear, pyroxene is dominant and talc is absent. Tremolite formation in this study is therefore occurring at conditions analogous to *P-T* region III of Maresch et al. (1994), where the assemblage is amphibole, diopside, enstatite, and quartz. Although Maresch et al. (1994) also observed intergrowths of amphibole with diopsidic pyroxene, there is a key

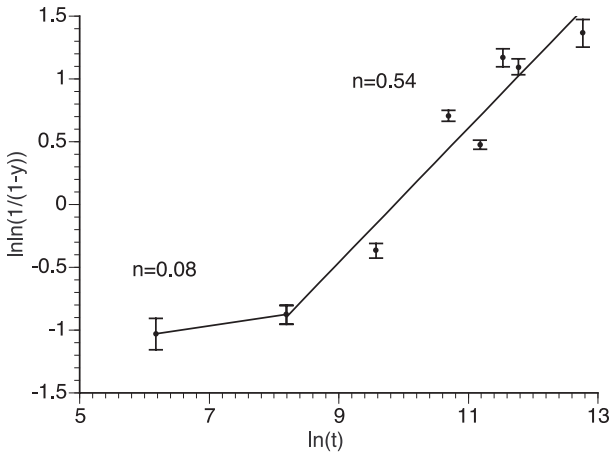

FIGURE 9. Plot of $\ln\ln[1/(1 - y)]$ vs. $\ln t$. The variable y is the concentration fraction of amphibole formed during the time-series experiments, and t is time in seconds. The slope of the curve changes considerably after the initial 1 h of reaction. The two straight-line regions conform to the Johnson–Mehl–Avrami equation with $n = 0.08$ and 0.54, respectively. The error bars represent the uncertainties in determination of the concentration

difference in the textural relationships between the amphibole and pyroxene. Maresch et al. (1994) noted that, in crystals where amphibole predominates over pyroxene, diopside lamellae are restricted to the core, and wide reaction fronts were observed where diopside lamellae transform to amphibole. Neither these wide reaction fronts nor the clear presence of amphibole armoring diopside cores was observed in this study.

Three general mechanisms of amphibole formation can be proposed that differ in the sequence of formation of the basic pyribole modules. The first mechanism involves a hydration process, where nucleation of mica-like modules occurs by the formation of hydrated, wide-chain (multiplicity ≥ 3) lamellae, followed by their breakdown to double-chain modules, incorporation of M4-type cations, and ordering into the amphibole structure. The second mechanism involves initial formation of pyroxene modules, with consequent hydration of the octahedral strips and rearrangement into the double-chain amphibole structure. The third mechanism is direct nucleation and growth of amphibole. Most likely, all three mechanisms operate concurrently during our experiments but with one particular mechanism being statistically the most favorable at a given time.

Indirect evidence for the first reaction mechanism can be found in the presence of wide-chain (particularly triple-chain) lamellae occurring in amphibole-rich hosts (Fig. 4), indicating some involvement of wide-chain lamellae with amphibole formation. However, conversion of triple-chain lamellae to double-chain amphibole, involving so-called "zipper" terminations, were generally not observed. Similarly, the presence of at least some amphibole crystals within the first 8 min of reaction provides evidence for the third reaction mechanism. These crystals suggest that direct precipitation of amphibole from a saturated solution is possible. Both the first and third mechanisms are probably subordinate, however, to the second reaction mechanism in the initial stages of reaction as supported by the following observations. First, pyroxenes are the dominant phases in the first 1 h of reaction. Second, the synthesis conditions used here are above the stability field of talc, so that wide-chain precursors are restricted to lamellae within other phases and do not appear as discrete phases (i.e., talc). In essence, this suggests that the vibrational energy of hydroxyl (OH^-) groups is too high to form stable nuclei of hydrated phases (amphibole or talc) and that the dominant reaction mechanism leads to pyroxene nucleation and growth. Third, HRTEM images document the intimate intergrowth of amphibole and pyroxene lamellae indicating a close genetic link between the two.

If the high vibrational energy of hydroxyl groups at these synthesis conditions is the primary factor limiting the rate of OH^- incorporation into the silicate chain modules, then a multiple-stage mechanism for amphibole formation is required. These stages are (1) formation of diopsidic pyroxene; (2) hydration and partial dissolution of diopside; and (3) nucleation and growth of amphibole accompanied by continued dissolution of diopside. The initially formed pyroxene crystals may trap a limited number of hydroxyl groups, thus providing a suitable environment for the formation of amphibole nuclei. The observed narrow (one half unit cell wide) amphibole lamellae nucleating within diopside support the above interpretation. With increasing synthesis duration, the numbers and sizes of amphibole nuclei created by this process of hydration increase. Dissolution of the pyroxene acts to enrich the proportion of amphibole in these pyroxene/hydrated-chain composites. The increased mass of these amphibole nanoparticles enables trapping of additional hydroxyl groups and facilitates their continued growth. After sufficiently large amphibole crystals have formed by this 3-stage pyroxene-to-amphibole conversion sequence listed above, the dominant growth mechanism becomes the direct precipitation of amphibole from solution onto these amphibole nuclei.

Enstatite does not appear to follow the same reaction mechanism as the diopsidic pyroxene. The presence of few CMFs, the absence of amphibole lamellae within its structure, and the rapid decline in the abundance of enstatite all suggest that enstatite, once formed, primarily decreases in abundance by dissolution rather than by topotactic conversion to amphibole. The correlation between the disappearance of the most Mg-rich amphiboles (Cm, Fig. 8b) and the nearly complete disappearance of enstatite (Table 1) after 20 h, suggests that dissolving enstatite leads to preferential precipitation of Mg-rich amphibole, and this process no longer occurs when enstatite is gone. Eventually, the Mg-rich amphibole (Cm and Cm-TrI) decreases in abundance, either by transforming to more Ca-rich amphibole by incorporation of Ca into its structure or by preferential dissolution and reprecipitation as a more Ca-rich amphibole.

Composition and structure

The consequences of the mechanism of amphibole growth proposed above are expressed in the defects and composition of the crystallizing amphibole. Because growth of amphibole is controlled by kinetic factors and the presence of precursor pyroxene, the amphibole compositions vary significantly. The hydration kinetics of single-chain modules largely controls the amphibole composition in the initial 20 to 30 h of crystallization. In the later growth stages, direct precipitation of amphibole

diminishes the spread in composition. Approach to the ultimate equilibrium composition is also a function of kinetic factors and depends on the conditions and duration of treatment.

Some of the Mg-rich amphiboles formed in the early stages of reaction have a primitive monoclinic structure, which results from incorporation of Mg at the M4 sites. Primitive cummingtonite occurs in nature (Robinson and Jaffe 1969; Ross et al. 1969; Rice et al. 1974; Immega and Klein 1976; Yakovleva et al. 1978; Robinson et al. 1982; Ghose 1982, Hirschmann et al. 1994, Yang and Hirschmann 1995), but in all cases it is ferromagnesian or manganoan cummingtonite with more than 10% Fe and/or Mn at the M4 sites. The only report of end-member primitive monoclinic cummingtonite, occurring as exsolution lamellae in tremolite, is that of Bown (1966). The primitive monoclinic cummingtonite synthesized in this study is apparently metastable because it disappears in the final stages of synthesis. It probably has not been described in previous synthesis studies because of its metastability, limited abundance, and because no other experiments with such short duration times as in the present study have been reported. Routine characterization of run products by XRD would not detect its presence, because of the general broadening of diffraction peaks due to small crystal size, variable composition (and cell dimensions), and defects, all of which are typical results of short synthesis experiments. Anthophyllite was not detected.

The composition of tremolitic amphibole as a function of pressure, temperature, and mineral assemblage is still a debated topic (e.g., Yang and Evans 1996; Gottschalk et al. 1999; Evans et al. 2000). The present study bears on this debate. As already shown, the most abundant structural defects in synthetic amphibole from these experiments are single- and triple-chain CMFs (Table 4). Although the compositional shift induced by these CMFs varies with experiment duration, the maximum Mg enrichment attributed to CMFs is equivalent to less than 5 mol% Cm component (Table 4). The low density of wide-chain CMFs can be explained by the mechanism of amphibole growth, which prevents formation of extended mica (or talc) type structural slabs. The Cm content of amphibole attributed to solid solution of Mg for Ca, i.e., not to CMFs, varies between 20 and 15 mol% in the first hour of crystallization. This value drops with time and after about 28 h reaches a steady state at approximately 6.3 to 7 mol%.

There now appears to be some degree of consistency among the most recent studies of tremolite synthesis. Zimmermann et al. (1996), who were able to grow relatively defect-free tremolitic amphibole at 2 kbar and 800 °C using concentrated brine solutions, observed a spread in the Ca/Mg ratios of 0.372 to 0.364 and an average amphibole composition equivalent to 5.5 mol% Cm content. Gottschalk et al. (1999), who also synthesized relatively defect-free tremolitic amphiboles in concentrated brines, reported Cm contents of 4 to 6 mol% for syntheses at 800 °C. Using the positive correlation between the Cm content and temperature reported by Gottschalk et al. (1999), these authors would predict Cm contents of 5 to 7 mol% at 850 °C, the synthesis temperature used in this study. Both of these studies reported somewhat lower Cm contents than the 10 mol% value reported by Jenkins (1987). The present study indicates that about 3 mol% of the Cm content results from CMFs, which, when applied to the study of Jenkins (1987), brings the Cm content caused by solid solution of Mg for Ca down to about 7 mol%. With this correction, all three studies cited above would yield a genuine Cm content of 5–7 mol% for tremolitic amphiboles synthesized in the range of 800–850 °C.

The principal question that remains is whether the true solid solution of about 6.3–7 mol% Cm observed in this study at 850 °C represents a thermodynamically stable composition for tremolitic amphibole, or is metastably preserved due to kinetic factors. For example, the thermodynamic treatment of Ghiorso and Evans (2002) indicates that tremolitic amphibole coexisting with diopside at 850 °C and 5 kbar should have a Ca/(Ca + Mg) ratio of 0.277, or about 3 mol% Cm. This value is a slightly lower Cm content than is observed in this study and would suggest that the present experiments have been kinetically inhibited from reaching the equilibrium composition. Experimentally, this may turn out to be an unsolvable problem that results from preferential growth of metastable pyroxene initially, which affects the composition and structure of the tremolite formed later, even for very long run times. Kinetic factors are certainly responsible for the Mg enrichment and large spread in Cm contents of tremolitic amphibole observed in the initial stages of growth (Table 3). The narrower compositional ranges for natural tremolite (e.g., Fig. 5 in Jenkins 1987) and the 6–7 mol% Cm component observed in this study for synthetic tremolite after prolonged treatments, suggest that there may be a local Gibbs free-energy minimum, metastable persistence at a tremolite-cummingtonite spinodal boundary, or entropy driven disordering (Hawthorne 1995) for Mg-enriched, tremolitic amphiboles. The driving force and kinetics for attaining the thermodynamically stable amphibole composition may simply be too weak and too sluggish to produce equilibrium on laboratory time scales.

ACKNOWLEDGMENTS

We thank Alison Pawley, Michael Czank, and an anonymous reviewer for their constructive and critical reviews, which improved the quality of this paper. Thanks go to Joshua Sandberg for digitizing the XRD patterns. This research was supported by NSF grants EAR–9418090 and EAR-0073955 to D.R.V. and EAR-9909452 to D.M.J., which the authors gratefully acknowledge.

REFERENCES CITED

Ahn, J.H., Cho, M., Jenkins, D.M., and Buseck, P.R. (1991) Structural defects in synthetic tremolitic amphiboles. American Mineralogist, 76, 1811–1823.

Aranovich, L.Y. and Newton, R.C. (1999) Experimental determination of CO_2-H_2O activity-composition relations at 600–1000 °C and 6–14 kbar by reversed decarbonation and dehydration reactions. American Mineralogist, 84, 1319–1332.

Borg, I.Y. and Smith, D.K. (1969) Calculated X-ray powder patterns for silicate minerals. Geological Society of America Memoir, 122, 896 p.

Bown, M.G. (1966) A new amphibole polymorph in intergrowth with tremolite: clinoanthophyllite. American Mineralogist, 51, 259–260.

Boyd, F.R. (1959) Hydrothermal investigations of amphiboles. In P.H. Abelson, Ed., Researches in Geochemistry, p. 377–396. Wiley, New York.

Bozhilov, K.N., Jenkins, D.M., and Veblen, D.R. (1993) TEM/AEM observations of chain silicate evolution during synthesis of tremolite. Transactions of the American Geophysical Union (EOS), 74 Supplement, 166.

———(1994) Reaction mechanism for tremolite formation from diopside + enstatite + quartz + H_2O. Geological Society of America Abstracts with Programs, 26, A-261.

Chernosky, J.V. Jr., Berman, R.G., and Jenkins, D.M. (1998) The stability of tremolite: New experimental data and a thermodynamic assessment. American Mineralogist, 83, 726–738.

Christian, J.W. (1975) Transformations in metals and alloys. I. Equilibrium and general kinetic theory. Pergamon Press, Oxford.

Evans, B.W., Ghiorso, M.S., and Kuehner, S.M. (2000) Thermodynamic properties of tremolite: A correction and some comments. American Mineralogist, 85, 466–472.

Fiori, C.E., Swyt, C.R., and Myklebust, R.L. (1994) DTSA: Desk top spectrum analyzer and x-ray data base. National Institute of Standard and Technology, Gaithersburg, MD.
Ghiorso, M.S. and Evans, B.W. (2002) Thermodynamics of the amphiboles: Ca-Mg-Fe^{2+} quadrilateral. American Mineralogist, 87, 79–98.
Ghose, S. (1982) Mg-Fe disorder in ferromagnesian silicates. In S.K. Saxena, Ed., Advances in physical geochemistry, p. 1–57. Springer-Verlag, New York.
Gottschalk, M., Andrut, M., and Melzer, S. (1999) The determination of the cummingtonite content of synthetic tremolite. European Journal of Mineralogy, 11, 967–982.
Graham, C.M., Maresch, W., Welch, M.D., and Pawley, A.R. (1989) Experimental studies on amphiboles: A review with thermodynamic perspectives. European Journal of Mineralogy, 1, 535–555.
Hawthorne, F.C. (1983) The crystal chemistry of the amphiboles. Canadian Mineralogist, 21, 173–480.
———(1995) Entropy-driven disorder in end-member amphiboles. Canadian Mineralogist, 33, 1189–1204.
Hawthorne, F.C. and Grundy, H.D. (1976) The crystal chemistry of the amphiboles: IV. X-ray and neutron refinements of the crystal structure of tremolite. Canadian Mineralogist, 14, 334–345.
Hewitt, D.A. (1975) Stability of the assemblage phlogopite-calcite-quartz. American Mineralogist, 60, 391–397.
Hirschmann, M.E., Evans, B.W., and Yang, H. (1994) Composition and temperature dependence of Fe-Mg ordering in cummingtonite—grunerite as determined by X-ray diffraction. American Mineralogist, 79, 862–877.
Hutchison, J.L., Irusteta, M.C., and Whittaker, E.J.W. (1975) High-resolution electron microscopy and diffraction studies of fibrous amphiboles. Acta Crystallographica, A31, 794–801.
Immega, I.P. and Klein, C., Jr. (1976) Mineralogy and petrology of some metamorphic Precambrian iron-formations in southwestern Montana. American Mineralogist, 61, 1117–1144.
Jenkins, D.M. (1983) Stability and composition relations of calcic amphiboles in ultramafic rocks. Contributions to Mineralogy and Petrology, 83, 375–384.
———(1987) Synthesis and characterization of tremolite in the system H_2O-CaO-MgO-SiO_2. American Mineralogist, 72, 707–715.
Jenkins, D.M. and Clare, A.K. (1990) Comparison of the high-temperature and high-pressure stability limits of synthetic and natural tremolite. American Mineralogist, 75, 358–366.
Jenkins, D.M., Holland, T.J.B., and Clare, A.K. (1991) Experimental determination of the pressure-temperature stability field and thermochemical properties of synthetic tremolite. American Mineralogist, 76, 458–469.
Kiseleva, I.A. and Ogorodova, L.P. (1984) High-temperature solution calorimetry for determining the enthalpies of formation for hydroxyl-containing minerals such as talc and tremolite. Geochemistry International, 12, 36–46.
Lager, G.A., Jorgensen, J.D., and Rotella, F.J. (1982) Crystal structure and thermal expansion of α-quartz SiO_2 at low temperatures. Journal of Applied Physics, 53, 6751–6756.
Levien, L. and Prewitt, C.T. (1981) High-pressure structural study of diopside. American Mineralogist, 66, 315–323.
Livi, K.J.T. and Veblen, D.R. (1987) "Eastonite" from Easton, Pennsylvania: A mixture of phlogopite and a new form of serpentine. American Mineralogist, 72, 113–125.
Maresch, W.V. and Czank, M. (1983) Phase characterization of synthetic amphiboles on the join $Mn_x^{2+}Mg_{7-x}[Si_8O_{22}](OH)_2$. American Mineralogist, 68, 744–753.
Maresch, W.V. and Czank, M. (1988) Crystal-chemistry, growth-kinetics and phase-relationships of structurally disordered (Mn^{2+},Mg)-amphiboles. Fortschritte der Mineralogie, 66, 69–121.
Maresch, W.V., Czank, M., and Schreyer, W. (1994) Growth mechanism, structural defects and composition of synthetic tremolite: What are the effects on macroscopic properties? Contributions to Mineralogy and Petrology, 118, 297–313.
Metz, P. (1967) Experimentelle Bildung von Forsterit und Calcit aus Tremolit und Dolomit. Geochimica et Cosmochimica Acta, 31, 1517–1532.
Metz, P. (1976) Experimental investigation of the metamorphism of siliceous dolomites III. Equilibrium data for the reaction: 1 tremolite + 11 dolomite = 8 forsterite + 13 calcite + 9 CO_2 + 11 H_2O for the total pressure of 3000 and 5000 bars. Contributions to Mineralogy and Petrology, 58, 137–148.
Pawley, A.R., Graham, C.M., and Navrotsky, A. (1993) Tremolite-richterite amphiboles: Synthesis, compositional and structural characterization, and thermochemistry. American Mineralogist, 78, 149–156.
Rice, J.M., Evans, B.W., and Trommsdorff, V. (1974) Widespread occurrence of magnesio-cummingtonite, Cima di Gagnone, Ticino, Switzerland. Contributions to Mineralogy and Petrology, 43, 245–251.
Robie, R.A. and Stout, J.W. (1963) Heat capacity from 12 to 305 K, and entropy of talc and tremolite. Journal of Physical Chemistry, 67, 2252–2256.
Robinson, P. and Jaffe, H.W. (1969) Chemographic explanation of amphibole assemblages from central Massachusetts and southwestern New Hampshire. Mineralogical Society of America Special Paper, 2, 251–274.
Robinson, P., Spear, F.S., Schumacher, J.C., Laird, J., Klein, C., Evans, B.W., and Doolan, B.L. (1982) Phase relations of metamorphic amphiboles: Natural occurrence and theory. In D.R. Veblen and P.H. Ribbe, Eds., Amphiboles: Petrology and Experimental Phase Relations. Mineralogical Society of America Reviews in Mineralogy, 9B, 1–227.
Ross, M., Papike, J.J., and Shaw, K.W. (1969) Exsolution textures in amphiboles as indicators of subsolidus thermal histories. Mineralogical Society of America Special Paper, 2, 275–299.
Sasaki, S., Takeuchi, Y., Fujino, K., and Akimoto, S. (1982) Electron-density distributions of three orthopyroxenes, $Mg_2Si_2O_6$, $Co_2Si_2O_6$, $Fe_2Si_2O_6$. Zeitschrift für Kristallographie, 158, 279–297.
Skippen, G. and McKinstry, B.W. (1985) Synthetic and natural tremolite in equilibrium with forsterite, enstatite, diopside, and fluid. Contributions to Mineralogy and Petrology, 89, 256–262.
Snyder, R.L. and Bish, D.L. (1989) Quantitative analysis. In D.L. Bish and J.E. Post, Eds., Modern powder diffraction, 20, 101–144. Reviews in Mineralogy, Mineralogical Society of America, Washington, D.C.
Stadelmann, P. (1987) EMS—a software package for electron diffraction analysis and HRTEM image simulation in materials science. Ultramicroscopy, 21, 131–146.
Thompson, J.B. Jr. (1978) Biopyriboles and polysomatic series. American Mineralogist, 63, 239–249.
———(1981) An introduction to the mineralogy and petrology of the biopyriboles. In D.R. Veblen, Ed., Amphiboles and Other Hydrous Pyriboles—Mineralogy, 9A, 141–188. Reviews in Mineralogy, Mineralogical Society of America, Washington, D.C.
Troll, G. and Gilbert, M.C. (1972) Fluorine-hydroxyl substitution in tremolite. American Mineralogist, 57, 1386–1404.
Veblen, D.R. (1981) Non-classical pyriboles and polysomatic reactions in biopyriboles. In D. R. Veblen, Ed., Amphiboles and Other Hydrous Pyriboles—Mineralogy, 9A, 189–236. Reviews in Mineralogy, Mineralogical Society of America, Washington, D.C.
Veblen, D.R., Buseck, P.R., and Burnham, C.W. (1977) Asbestiform chain silicates: new minerals and structural groups. Science, 198, 359–365.
Welch, M.D. (1987) Experimental studies of amphiboles in the system Na_2O-CaO-MgO- Al_2O_3-SiO_2-H_2O-SiF_4 and its subsystems. Ph.D. thesis, University of Edinburgh, U.K.
Welch, M.D. and Pawley, A.R. (1991) Tremolite: New enthalpy and entropy data from a phase equilibrium study of the reaction tremolite = 2 diopside + 1.5 orthoenstatite + β-quartz + H_2O. American Mineralogist 76, 1931–1939.
Yakovleva, A.K., Yegorova, L.N., and Litvin, A.L. (1978) Magnesiocummingtonite with primitive cell $P2_1/m$. International Geological Review, 20, 1357–1362.
Yang, H. and Evans, B.W. (1996) X-ray structural refinements of tremolite at 140 and 295K: Crystal chemistry and petrologic implications. American Mineralogist, 81, 1117–1125.
Yang, H. and Hirschmann, M.M. (1995) Crystal structure of $P2_1/m$ ferromagnesian amphibole and the role of cation ordering and composition in the $P2_1/m$-$C2/m$ transition in cummingtonite. American Mineralogist, 80, 916–922.
Yin, H.A. and Greenwood, H.J. (1983) Displacement of equilibria of OH-tremolite and F-tremolite solid solution. I. Determination of the equilibrium *P-T* curve of OH-tremolite. Transactions of the American Geophysical Union (EOS), 64, 347.
Young, R.A., Sakthivel, A. Moss, T.S., and Paiva-Santos, C.O. (1995) DBWS-9411, an upgrade of the DBWS*.* programs for Rietveld refinement with PC and mainframe computers. Journal of Applied Crystallography, 28, 366–367.
Zimmerman, R., Heinrich, W., and Franz, G. (1996) Tremolite synthesis from $CaCl_2$-bearing aqueous solutions. European Journal of Mineralogy, 8, 767–776.

MANUSCRIPT RECEIVED FEBRUARY 17, 2003
MANUSCRIPT ACCEPTED JUNE 18, 2003
MANUSCRIPT HANDLED BY ALISON PAWLEY